

Research Article

Computational Screening of Ca-Containing Coating Materials for Electrodes of Ca-Ion Batteries

Myeongjun Kim and Haesun Park

School of Integrative Engineering, Chung-Ang University, 84, Heukseok-ro, Dongjak-gu, Seoul 06974, Republic of Korea

Correspondence should be addressed to Haesun Park; parkh@cau.ac.kr

Received 17 November 2023; Revised 27 May 2024; Accepted 12 June 2024

Academic Editor: Suresh Kannan Balasingam

Copyright © 2024 Myeongjun Kim and Haesun Park. This is an open access article distributed under the Creative Commons Attribution License, which permits unrestricted use, distribution, and reproduction in any medium, provided the original work is properly cited.

The energy storage system utilizing calcium as a charge carrier is gaining prominence due to its abundance in the Earth's crust, reduction potential that is comparable to lithium ($\text{Li}/\text{Li}^+ = -3.04\text{ V}$, $\text{Ca}/\text{Ca}^{2+} = -2.84\text{ V}$), and its nontoxic nature. Enabling practical Ca-ion batteries demands overcoming challenges in forming both electrically nonconductive and ionically conductive SEI layers. We propose a coating strategy and thermodynamic screening via the Materials Project database to pinpoint suitable coating materials. Our selection criteria encompass phase stability, electronic properties, and electrochemical stability. Among 787 compounds, we identified 46 candidates (29 anodic, 24 cathodic, and 7 of them are on both sides) based on reduction/oxidation potential and width of the stability window. Optimal compounds such as $\text{Ca}_4\text{Cl}_6\text{O}$ and CaCN_2 for anodes, and $\text{Ca}(\text{AlCl}_4)_2$, CaCO_3 , CaSO_4 , KCaF_3 , and CaAlF_5 for cathodes exhibit superior interfacial stability for electrode coating, holding promise for Ca-ion batteries. This study can provide foundational insights into coating materials for Ca-ion batteries, offering guidance for electrode interface stabilization and practical battery design.

1. Introduction

The growing renewable energy production demands large-scale dispatchable energy storage systems [1, 2, 3]. While a Li-ion battery (LIB) is a promising system for grid energy storage, the limited Li reserves and surge in the number of electrified vehicles necessitate the development of beyond-Li-ion chemistry with high energy density at a low cost [4, 5]. Energy storage chemistries that harness multivalent ions have garnered considerable interest as promising candidates for beyond Li-ion chemistry, offering cost-effective solutions for high-voltage batteries.

Among the multivalent working cations, an emerging energy storage system utilizes Ca as a charge carrier. Ca is the fifth most abundant material on Earth, leading to a lower price than LIB [6]. Besides its abundance, the multivalency of Ca allows a higher charge density than monovalent ions because, for the same charge, the redox reaction requires only half the number of Ca ions [7, 8]. Furthermore, the reduction potential of Ca, comparable to Li ($\text{Li}/\text{Li}^+ = -3.04\text{ V}$, $\text{Ca}/\text{Ca}^{2+} = -2.84\text{ V}$), results in higher cell voltage and capacity

than other multivalent counterparts, such as Mg ($\text{Mg}/\text{Mg}^{2+} = -2.37\text{ V}$) or Zn ($\text{Zn}/\text{Zn}^{2+} = -0.76\text{ V}$). Moreover, the less polarizing character (charge/radius ratio) of Ca^{2+} ions results in higher ionic mobility in liquid electrolytes than Mg^{2+} and Al^{3+} ions [6]. These distinct advantages of Ca-ion batteries offer promising and sustainable long-term solutions for large-scale energy storage [7, 9, 10, 11, 12].

However, the development of Ca-ion batteries is at a nascent stage, and a significant challenge lies in the poor interfacial stability between the Ca electrode and electrolyte [13, 14, 15, 16]. An example of Ca metal solid–electrolyte interface (SEI) is CaCl_2 , exhibiting extremely low Ca diffusivity, causing limited reversibility of the cell [14, 15, 16]. One common strategy to enhance interfacial stability introduces an artificial SEI that prevents direct contact between the electrode/electrolyte and forms an undesirable passivating layer [17, 18, 19, 20, 21, 22]. Implementing an artificial SEI layer is a widely employed strategy to enhance the interfacial stability between active materials and electrolytes. Using high-throughput computational screening, researchers have successfully identified coating candidates

demonstrating enhanced interfacial stability in Li, Na, K, and Mg battery systems [23, 24].

Furthermore, Jeong et al. [25] incorporated an Al_2O_3 coating layer into the silicon-based anodes of all-solid-state LIBs, based on the thermodynamic screening results of Li–Al–O coating materials conducted by Yu et al. [23] with the aim of enhancing cycle stability [19]. After undergoing 100 charge–discharge cycles, the half-cell with the Al_2O_3 coating demonstrated a discharge capacity of 502.08 mAh g^{-1} and a capacity retention ratio of 58.86% [23, 25]. This improvement, as observed when introducing a coating layer, underscores the importance of thermodynamic screening in enhancing the cycle properties of LIB systems. Our thermodynamic assessment serves as a criterion for selecting coating materials that can improve cycling performance, especially considering the significant degradation in cyclability caused by the strong reactivity of the Ca metal anode. Therefore, these results could provide a solid foundation for the successful implementation of Ca-ion batteries by introducing coating layers that ensure interfacial stability in calcium-ion batteries.

The study aimed to systematically screen 787 potential anode and cathode coating materials for application in Ca-ion batteries. The optimal coating materials for anodes and cathodes were identified by constructing grand potential phase diagrams using the Materials Project (MP) database. This identification ensures the maintenance of the electrochemical stability of the electrodes under battery operating conditions, where the chemical potential of the working cation fluctuates. Moreover, various binary and ternary compounds containing Ca were assessed, including fluorides, chlorides, oxides, sulfides, phosphides, and nitrides.

2. Computational Methods

The total energies of the compounds investigated in this study were obtained from the MP database [26]. These energies were evaluated using density functional theory calculations implemented in the Vienna Ab initio Simulation Package [27, 28]. The core–valence electron interactions were described by the projector-augmented wave potentials [29] and using the generalized gradient approximation formulated by Perdew–Burke–Ernzerhof [30]. An energy correction was applied to the anions, transition metals, and gas/liquid phases in the MP database to calculate the formation energies accurately [31, 32, 33, 34].

The electrochemical stability windows of each compound were calculated using the grand potential phase diagram, where the chemical potential μ_{Ca} is defined using the following equation [35]:

$$\mu_{\text{Ca}}(\varphi) = \mu_{\text{Ca},0} - e\varphi, \quad (1)$$

where $\mu_{\text{Ca},0}$ is the chemical potential of Ca metal, e is the elementary charge, and φ is the potential of the reference to the Ca metal anode. The chemical potential μ_{Ca} relates straight to the voltage vs. Ca/Ca^{2+} , which is expressed as follows:

$$V = -\frac{\mu_{\text{Ca}}}{zF}, \quad (2)$$

where F is the Faraday constant, z is the number of electrons transferred ($z = 2$ for Ca), and μ_{Ca} is referenced to the energy of Ca metal.

Python materials genomics (Pymatgen) was used to generate the grand potential phase diagram and identify stable compounds as a function of the chemical potential μ_{Ca} [31, 34]. This approach allowed us to effectively showcase the most stable phase(s) within each composition space as a function of the chemical potential μ_{Ca} by constructing a convex hull in the grand potential composition space. Detailed methods for constructing grand potential phase diagrams have been reported elsewhere [17, 35, 36].

The study began by collecting 44 binary and 743 ternary compounds that exhibited reasonable phase stability (convex hull less than 50 meV/atom). We only consider compounds with a nonzero bandgap to avoid the undesirable deposition of Ca on the coating/electrolyte interface. The set was then refined to 44 binary and 539 ternary compounds by constraining the anionic elements of the ternary compounds to fluorides, chlorides, oxides, sulfides, and nitrides. The grand potential phase diagram analysis was employed for the 44 binary and 539 ternary compounds to ascertain their electrochemical stability windows. Through this process, compounds that were unstable at any μ_{Ca} were identified and filtered, leading to the selection of 244 compounds (218 ternaries and 26 binaries) for further consideration. Finally, from the selected 244 compounds, the cathode and anode coating materials for Ca-ion batteries were screened, considering the voltage variations of the electrodes during battery operation. The electrochemical stability windows of all 244 compounds are listed in Table S1. The reduction potential of prospective anode coating materials was lower than 0.3 V, and the width of the stability window was larger than 1 V. The value, 0.3 V, was based on an earlier investigation of Li_3BO_3 coatings, revealing that Li_3BO_3 does not react with a Li metal anode, attributed to the sluggish kinetics, despite possessing a reduction potential of +0.27 V [14]. For cathode coating materials, materials with an oxidative potential lower than 4 V and a reduction potential higher than 2 V were excluded. In addition, prospective cathode-coating compounds exhibited stability windows wider than 2.0 V.

3. Results and Discussion

Figure 1 illustrates the stability windows of the Ca-containing binaries, evaluated using a grand potential phase diagram. Among the 44 compounds containing Ca, except unstable compounds at any μ_{Ca} , 26 compounds are selected. The electrochemical stability windows of the 11 binary compounds satisfying the criteria for cathode and anode coatings are shown in Figure 1. The zero on the voltage axis (y -axis) was referenced to the bulk Ca metal (V vs. Ca/Ca^{2+}). The binary compounds, except CaB_6 and CaMg_{149} , were stable at 0 V, indicating that the binaries are promising coating materials

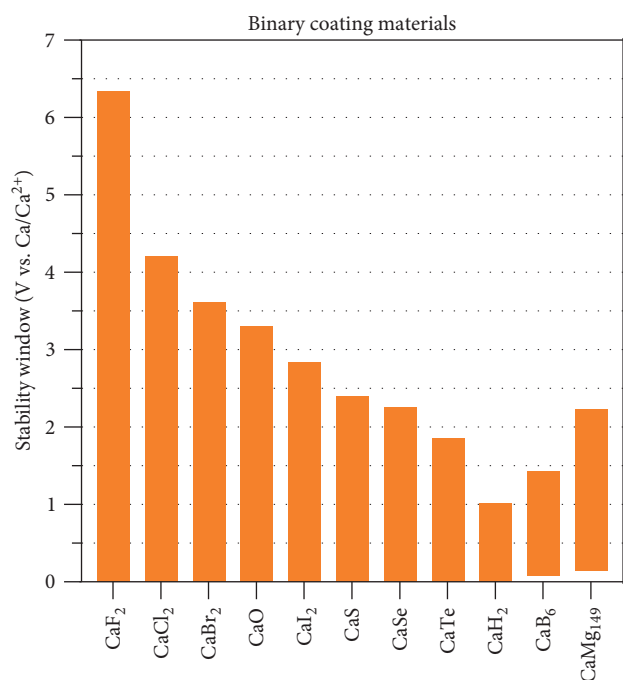


FIGURE 1: The electrochemical stability windows of calcium-containing binaries. The lower and upper limits of the orange bars represent the reductive and oxidative potentials, respectively.

for Ca metal anodes in direct contact with the Ca metal anode. Although CaB₆ and CaMg₁₄₉ were not stable at 0 V vs. Ca/Ca²⁺, the reduction potentials of each compound were 0.08 and 0.13 V, respectively, slightly higher than 0 V. Given that the reduction potential of Li₇La₃Zr₂O₁₂ (LLZO) was only 0.05 V vs. Li/Li⁺ and LLZO formed a relatively stable interface with Li metal, CaB₆ and CaMg₁₄₉ could be applied to Ca metal coating materials [17]. Moreover, the reduction potentials of these two Ca binaries were lower than those of another promising Ca anode material, CaSi₂, which has a reduction potential of 0.8 V vs. Ca/Ca²⁺, suggesting CaB₆ and CaMg₁₄₉ can be exploited for coating materials of CaSi₂ alloying anode [37].

All halide and chalcogenide binary compounds exhibited stability at 0 V, affirming their effectiveness as Ca anode-coating materials due to their stable contact with the Ca metal anode. Halides generally have higher oxidation potentials than chalcogenides. For instance, the oxidation potentials of CaF₂, CaCl₂, and CaBr₂ are 6.3, 4.2, and 3.6 V, respectively, indicating its feasibility as a coating material for high-voltage cathodes. Conversely, halides with lower oxidation potentials than chalcogenides make them suitable for low-voltage cathodes. The superior oxidative stability of chalcogenides over halides is consistent with other binary for halides and chalcogenides compounds based on Li, Na, K, and Mg [23, 24].

Figure 2 illustrates the reduction and oxidation potentials of Ca ternary compounds. The points in Figure 2(a) are color-coded based on the type of anionic component they represent (blue for fluorides, red for chlorides, green for oxides, yellow for sulfides, and purple for nitrides). The dataset contained 28 fluoride compounds, 15 chlorides, 106 oxides, 10 sulfides, and

59 nitrides. Figure 2(b) illustrates the approximate location of each compound in the graph according to its anionic components. Here, the 0 V reduction potential indicates stable contact between the coating materials and Ca metal without implying that the coating materials are reduced at this potential.

The compounds in the upper-right corner of Figure 2(a) exhibit lower reduction and higher oxidation potentials, making them potential candidates for coating materials with a wide stability window. The compounds positioned close to the right y-axis (stable at 0 V) are suitable anodic coating materials. Compounds located on the upper side with an appropriate reduction potential (<2 V) are considered promising for cathode coating.

Most nitrides have a reduction potential lower than 0.8 V, yet they tend to exhibit poor oxidative stability (<2.2 V). For sulfides, only a few compounds are stable under 0.8 V, and their oxidation potentials range from 2 to 2.7 V. Consequently, nitride- and sulfide-based components are not suitable as coating cathodes but as anodes.

The electrode coating materials, fluorides, chlorides, and oxides, demonstrate superior performance compared with nitrides and sulfides. Fluorides (blue points) demonstrated a wide dispersion of reduction potentials ranging from 0.3 to 5.8 V. Chlorides (red points) and oxides (green points) also displayed a broad distribution of reduction potentials (ranging from 0 to 3.7 V), albeit not as extensive as that of fluorides. Despite their lower oxidation potentials than fluorides, some were still suitable as cathode coating materials, with oxidation potentials reaching 5.2 V.

In Figure 3, we categorize the evaluated compounds as coating materials for the cathode and anode because their required criteria differ significantly, making it feasible to have separate coatings on each side. The distinct characteristics and performance requirements of cathode and anode coatings necessitate a tailored approach to enhance the overall performance and stability of battery systems. The coating composition for each electrode can be optimized by carefully selecting materials based on their reduction and oxidation potentials.

The compounds depicted in Figure 3(a) show promise as anode coatings. The reduction potentials remained stable up to 0.3 V, and their oxidative limit was greater than 1 V. Notably, compounds with reduction potentials lower than 0.3 V were considered slow kinetic compounds, setting the maximum reduction potential for anode coating at 0.3 V [14]. The oxide ternary satisfying the criterion for anode coating includes Ca₄Cl₆O, CaSc₂O₄, and CaHfO₃. In addition, several chlorides (Ca₃PbCl₃, Ca₃AsCl₃, CaHCl, KCaCl₃, RbCaCl₃, CsCaCl₃, Cs₃Ca₂Cl₇, and Cs₂CaCl₄) and nitrides (Ca (BeN)₂, CaZrN₂, CaHfN₂, Ca₂TaN₃, Ca₂VN₃, CaCN₂, and Ca₂PN₃) exhibit superior reductive stabilities. For KCaCl₃, RbCaCl₃, CsCaCl₃, Cs₃Ca₂Cl₇, and Cs₂CaCl₄, their oxidative limits extended over 4 V, highlighting their versatility across both anode and cathode coatings.

The stability windows for the compounds suitable for cathode coating are depicted in Figure 3(b). The selection criteria included a reductive limit below 2.0 V and an oxidative limit

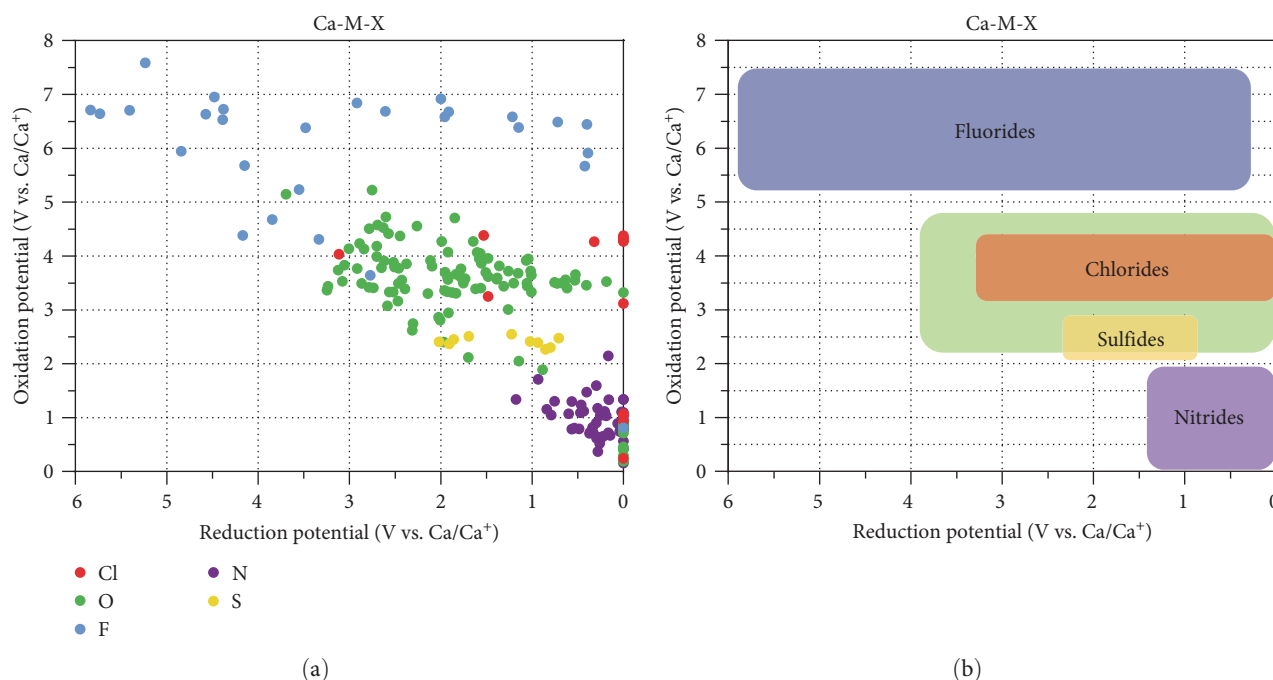


FIGURE 2: (a) Oxidation and reduction potential of 218 Ca ternaries. The blue, red, green, and yellow points represent fluorides, chlorides, oxides, and sulfides, respectively. (b) Approximate distribution of oxidation potential and reduction potential for Ca ternaries. They are grouped into rectangles according to their anionic components.

exceeding 4.0 V. The ternaries that comply with the specified criteria comprise oxides ($\text{CaTa}_4\text{O}_{11}$, CaCO_3 , $\text{Ca}(\text{B}_3\text{O}_5)_2$, CaSO_4 , CaMoO_4 , and $\text{Ca}_2\text{P}_2\text{O}_7$), chlorides ($\text{Ca}_2\text{P}_2\text{O}_7\text{KCaCl}_3$, RbCaCl_3 , CsCaCl_3 , $\text{Cs}_3\text{Ca}_2\text{Cl}_7$, Cs_2CaCl_4 , and $\text{Ca}_9\text{La}_5\text{Cl}_{33}$), and fluorides (KCaF_3 , CsCaF_3 , RbCaF_3 , Cs_2CaF_4 , CaAlF_5 , CaZrF_6 , CaTiF_6 , CaTaF_7 , and CaB_2F_8). Among these, chlorides and fluorides demonstrate superior reductive stabilities compared to oxides, with fluorides displaying the broadest stability window. Figure 3(b) does not include data on sulfides and nitrides because their oxidative stability is inadequate as a coating material between the cathode and the electrolyte.

Figure 4 illustrates the reduction/oxidation potential in relation to the proportion of the anionic component (A%), accompanied by the corresponding ternary phase diagram to correlate the reduction/oxidation potential of the ternary coating materials with their chemical compositions. The A% was calculated by dividing the number of anionic components by the total number of atoms in the chemical formula. For example, the A% of $\text{Ca}(\text{B}_3\text{O}_5)_2$ was 0.59, where the number of oxygen atoms was 10, and the total number of atoms was 17. The reduction and oxidation potentials were proportional to the A% for the Ca–B–O, Ca–P–O, Ca–Sn–O, and Ca–Si–O ternary systems. A similar tendency was observed for Li–Al–O, Li–Si–O, and Li–B–O ternary systems [24].

A high-throughput screening was performed to identify promising coating materials for the anodes and cathodes within Ca-ion batteries. The selection criteria and the number of remaining compounds after each screening step are shown in Figure 5. Initially, binary and ternary calcium-containing compounds were obtained from the MP database. The materials with low stability ($E^{\text{hull}} > 50 \text{ meV/atom}$) and

those with zero bandgap were excluded, resulting in 787 compounds. The selection process was further streamlined to 44 binary and 539 ternary compounds by restricting the anionic elements of the ternary compounds to fluorides, chlorides, oxides, sulfides, and nitrides. Furthermore, a chemical-potential-dependent phase diagram was constructed to exclude compounds exhibiting instability at any Ca chemical potential, leaving 244 compounds. Finally, we measured the electrochemical windows of these 244 compounds and identified the optimal coating materials for the anode and cathode. The anode coating materials were selected based on the reduction potential limit lower than 0.3 V and a stability window wider than 1 V. Cathode coating materials were selected based on oxidation limits higher than 4 V and reduction limits lower than 2 V. This screening procedure yielded 46 optimal compounds for the anode (29 compounds) and cathode (24 compounds) coatings. Among these 46 compounds, 7 satisfied the criteria for both anodes and cathodes. Refining our selection to include only lightweight, transition-metal-free, and potentially low-cost compositions identifies KCaCl_3 , $\text{Ca}_4\text{Cl}_6\text{O}$, and CaCN_2 as optimal anode coatings, and $\text{Ca}(\text{AlCl}_4)_2$, CaCO_3 , CaSO_4 , and KCaF_3 as optimal cathode coatings.

4. Conclusions

Prior studies have focused on pinpointing optimal coating materials for Li-ion, K-ion, Na-ion, and Mg-ion batteries by examining their thermodynamic properties, specifically through the evaluation of binary and ternary compounds to determine stability windows [23, 24]. Yet, similar research endeavors for calcium-ion batteries remain scarce, creating obstacles in the identification of appropriate coating

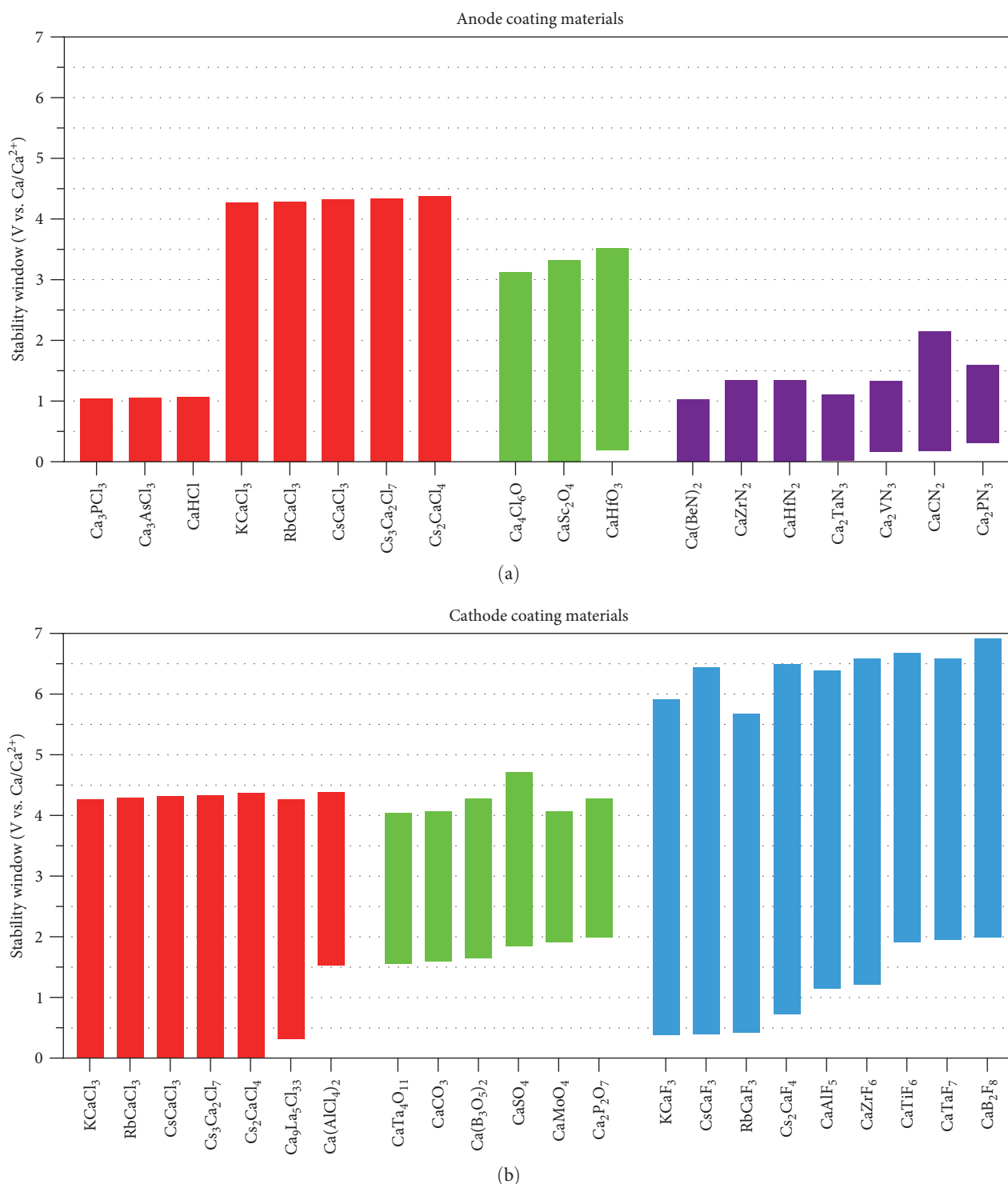


FIGURE 3: The electrochemical windows of prospective coating materials for (a) anode and (b) cathode of Ca-ion batteries. The red, green, purple, and blue represent chlorides, oxides, nitrides, and fluorides, respectively.

compounds. To enable the practical implementation of Ca-ion batteries, it becomes imperative to address the challenges hindering the formation of nonconductive SEI while simultaneously regulating the formation of conductive Ca-ion SEI. To address these issues, we propose the utilization of a coating

methodology, and in this investigation, we perform thermodynamic screening to identify potential coating materials.

Utilizing the MP data set, we selected CIB electrode coating materials according to the criteria outlined in Figure 5. Potential coating materials are expected to demonstrate

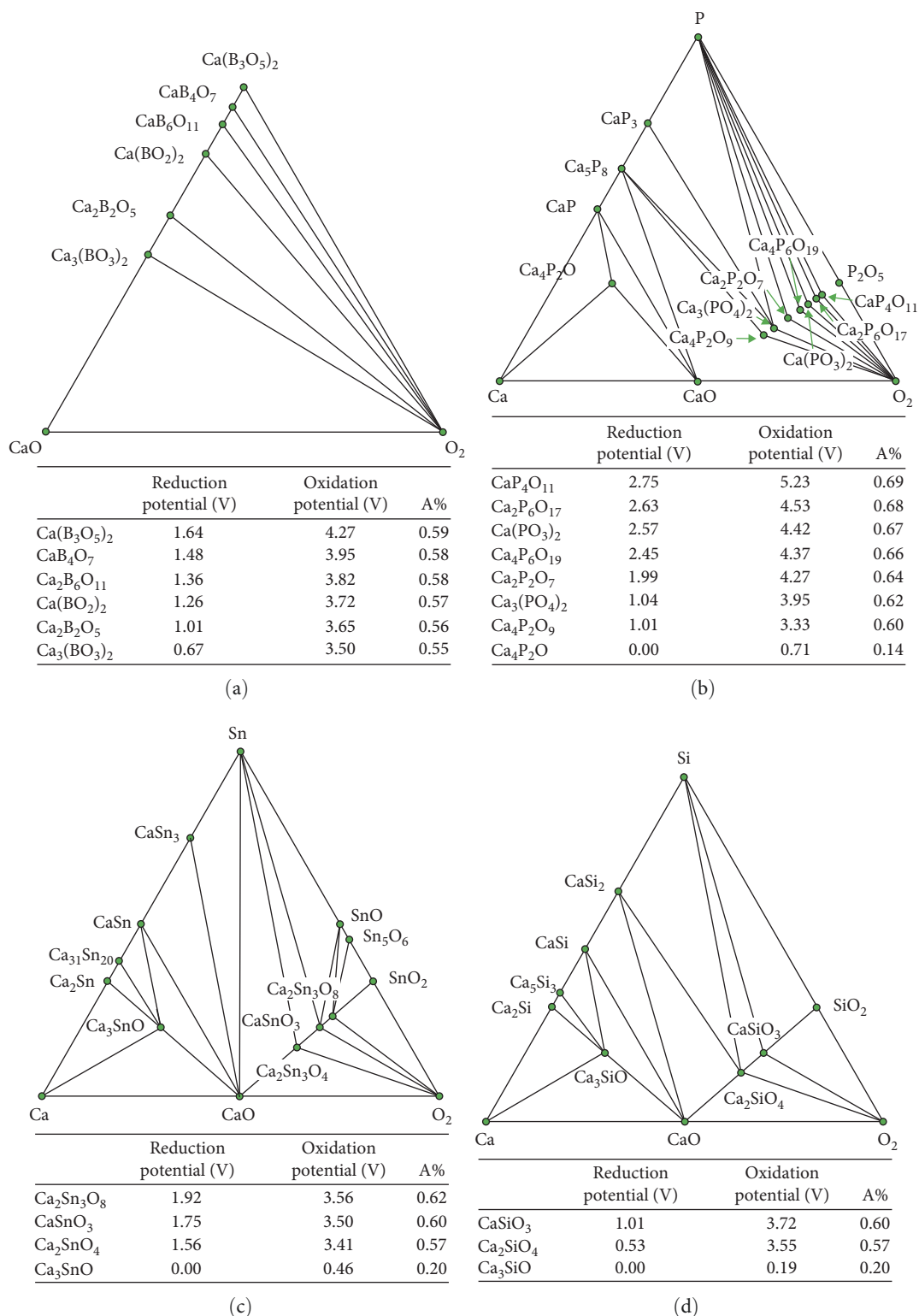


FIGURE 4: Phase diagram of (a) Ca-B-O, (b) Ca-P-O, (c) Ca-Sn-O, and (d) Ca-Si-O systems and oxidation and reduction potential of each compound with the proportion of anionic component (A%).

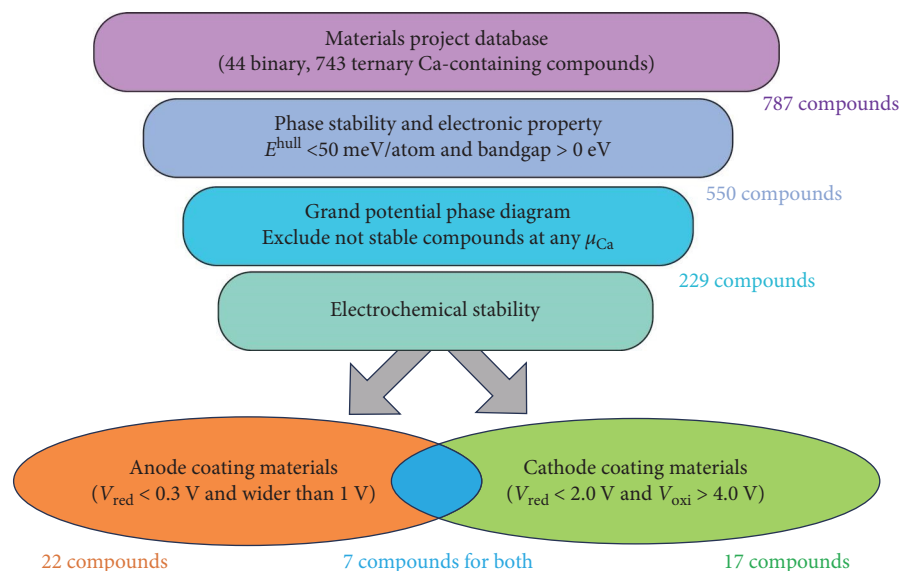


FIGURE 5: The criteria used in the high-throughput screening process and the number of compounds selected at each step of screening.

suitable phase stability, appropriate electronic properties ($E^{\text{hull}} < 50 \text{ meV/atom}$ and bandgap $> 0 \text{ eV}$), and exhibit stability within the grand potential phase diagram analysis. Within the materials that meet the aforementioned conditions, compounds exhibiting a reduction potential below 0.3 V and a stability window exceeding 1 V hold promise as potential anodic coating materials, and compounds displaying stability within the range of 2–4 V emerge as favorable candidates for cathode coating applications. In these criteria, a total of 46 candidate materials (29 for the anodic side and 24 for the cathodic side) were meticulously chosen as potential coating candidates from a pool of 787 compounds. Chlorides, oxides, and nitrides are stable between Ca metal anode and electrolyte. Among them, $\text{Ca}_4\text{Cl}_6\text{O}$ and CaCN_2 are the most optimal compounds, characterized by their lightweight, transition-metal-free, ease of synthesis, and potentially cost-effective compositions. Chlorides, oxides, and fluorides are stable between electrolyte and cathode. $\text{Ca}(\text{AlCl}_4)_2$, CaCO_3 , CaSO_4 , KCaF_3 , and CaAlF_5 show a wide range of stability windows, and they are economical candidates for coating the cathodic side of Ca metal batteries, being lightweight, synthesizable, and free from transition metals.

This study contributes essential foundational insights into the utility and performance enhancement of coating materials for Ca-ion batteries. The findings from this investigation on coating could provide design guidelines to stabilize the interface of electrodes of Ca-ion batteries. However, further consideration of ionic and electronic transport properties is essential to fully understand and rigorously screen coating materials. Our initial screening process focuses on compounds with nonzero bandgaps to minimize undesirable Ca deposition at the coating/electrode interface. Recent reports indicate that electrode coating materials typically have thicknesses ranging from approximately 5–50 nm [18, 38, 39]. Such ultra-thin coatings do not strictly require high ionic conductivity. Nevertheless, a comprehensive understanding of the electronic/ionic transport properties and their

correlation with interfacial stability between the coating and the electrode is crucial. Future research will involve simulating the transport properties of coating materials known to stabilize the interface. This approach will enable us to explore the correlation between these properties and interfacial stability. These studies could significantly enhance our understanding of the relationship between transport behavior and interface stability, leading to more rational and effective interface designs.

Data Availability

Reduction and oxidation potential data are available in the Supplementary Materials.

Conflicts of Interest

The authors declare no competing financial interest.

Acknowledgments

This research was supported by the Chung-Ang University Research Grants in 2021, and a National Research Foundation of Korea (NRF) grant funded by the Korea Government (MSIT) (NRF-2022R1C1C1011660).

Supplementary Materials

Table S1: electrochemical stability window of Ca containing 26 binaries and 218 ternaries. (*Supplementary Materials*)

References

- [1] L.-F. Wang, M.-M. Geng, X.-N. Ding et al., “Research progress of the electrochemical impedance technique applied to the high-capacity lithium-ion battery,” *International Journal of Minerals, Metallurgy and Materials*, vol. 28, no. 4, pp. 538–552, 2021.

- [2] A. Manthiram, B. Song, and W. Li, "A perspective on nickel-rich layered oxide cathodes for lithium-ion batteries," *Energy Storage Materials*, vol. 6, pp. 125–139, 2017.
- [3] A. Manthiram, "A reflection on lithium-ion battery cathode chemistry," *Nature Communications*, vol. 11, no. 1, 2020.
- [4] D. D. Sarma and A. K. Shukla, "Building better batteries: a travel back in time," *ACS Energy Letters*, vol. 3, no. 11, pp. 2841–2845, 2018.
- [5] M. Winter, B. Barnett, and K. Xu, "Before Li ion batteries," *Chemical Reviews*, vol. 118, no. 23, pp. 11433–11456, 2018.
- [6] M. E. Arroyo-de Dompablo, A. Ponrouch, P. Johansson, and M. R. Palacín, "Achievements, challenges, and prospects of calcium batteries," *Chemical Reviews*, vol. 120, no. 14, pp. 6331–6357, 2020.
- [7] J. Muldoon, C. B. Bucur, and T. Gregory, "Quest for nonaqueous multivalent secondary batteries: magnesium and beyond," *Chemical Reviews*, vol. 114, no. 23, pp. 11683–11720, 2014.
- [8] P. Canepa, G. Sai Gautam, D. C. Hannah et al., "Odyssey of multivalent cathode materials: open questions and future challenges," *Chemical Reviews*, vol. 117, no. 5, pp. 4287–4341, 2017.
- [9] A. Ponrouch and M. R. Palacín, "Post-Li batteries: promises and challenges," *Philosophical Transactions of the Royal Society A: Mathematical, Physical and Engineering Sciences*, vol. 377, no. 2152, Article ID 20180297, 2019.
- [10] K. M. Abraham, "Directions in secondary lithium battery research and development," *Electrochimica Acta*, vol. 38, no. 9, pp. 1233–1248, 1993.
- [11] B. Scrosati, "Lithium rocking chair batteries: an old concept?" *Journal of the Electrochemical Society*, vol. 139, no. 10, pp. 2776–2781, 1992.
- [12] J. M. Tarascon and D. Guyomard, "The $\text{Li}_{1+x}\text{Mn}_2\text{O}_4/\text{C}$ rocking-chair system: a review," *Electrochimica Acta*, vol. 38, no. 9, pp. 1221–1231, 1993.
- [13] A. Ponrouch, C. Frontera, F. Bardé, and M. R. Palacín, "Towards a calcium-based rechargeable battery," *Nature Materials*, vol. 15, no. 2, pp. 169–172, 2016.
- [14] E. Kazyak, K.-H. Chen, A. L. Davis et al., "Atomic layer deposition and first principles modeling of glassy $\text{Li}_3\text{BO}_3\text{-Li}_2\text{CO}_3$ electrolytes for solid-state Li metal batteries," *Journal of Materials Chemistry A*, vol. 6, no. 40, pp. 19425–19437, 2018.
- [15] E. Peled, A. Meitav, and M. Brand, "Calcium thionyl chloride high-rate reserve cell," *Journal of the Electrochemical Society*, vol. 128, no. 9, pp. 1936–1938, 1981.
- [16] A. Meitav and E. Peled, "Calcium—Ca (AlCl_4)²⁻—thionyl chloride cell: performance and safety," *Journal of The Electrochemical Society*, vol. 129, no. 3, pp. 451–457, 1982.
- [17] Y. Zhu, X. He, and Y. Mo, "Origin of outstanding stability in the lithium solid electrolyte materials: insights from thermodynamic analyses based on first-principles calculations," *ACS Applied Materials & Interfaces*, vol. 7, no. 42, pp. 23685–23693, 2015.
- [18] X. Han, Y. Gong, K. Fu et al., "Negating interfacial impedance in garnet-based solid-state Li metal batteries," *Nature Materials*, vol. 16, no. 5, pp. 572–579, 2017.
- [19] V. Pasala, S. Maddukuri, V. Sethuraman, R. Lankipalli, D. Gajula, and V. Manne, "Studies on multi-step addition of NMP in ($\text{LiNi}_{0.80}\text{Co}_{0.15}\text{Al}_{0.05}$) (NCA) cathode slurry preparation and its rheological, mechanical strength and electrochemical properties for Li-ion cells," *Journal of Electrochemical Science and Technology*, vol. 14, no. 3, pp. 262–271, 2023.
- [20] S. Kim, H. Kim, S. W. Doo et al., "One-step $\beta\text{-Li}_2\text{SnO}_3$ coating on high-nickel layered oxides via thermal phase segregation for Li-ion batteries," *Journal of Electrochemical Science and Technology*, vol. 14, no. 3, pp. 293–300, 2023.
- [21] M. J. Joo and Y. J. Park, "Stabilizing Li_2O -based cathode/electrolyte interfaces through succinonitrile addition," *Journal of Electrochemical Science and Technology*, vol. 14, no. 3, pp. 231–242, 2023.
- [22] C.-W. Kim, J. Choi, J.-H. Choi, J.-Y. Seo, and G. Park, " $\text{Zn}_3(\text{PO}_4)_2$ protective layer on Zn anode for improved electrochemical properties in aqueous Zn-ion batteries," *Journal of Electrochemical Science and Technology*, vol. 14, no. 2, pp. 162–173, 2023.
- [23] S. Yu, H. Park, and D. J. Siegel, "Thermodynamic assessment of coating materials for solid-state Li, Na, and K batteries," *ACS Applied Materials & Interfaces*, vol. 11, no. 40, pp. 36607–36615, 2019.
- [24] T. Chen, G. Ceder, G. Sai Gautam, and P. Canepa, "Evaluation of Mg compounds as coating materials in Mg batteries," *Frontiers in Chemistry*, vol. 7, 2019.
- [25] J. Jeong, K. Lee, C. Carpenter et al., "Improved cycle properties of all-solid-state Li-ion batteries with Al_2O_3 coating on the silicon-based anode," *Journal of Energy Engineering*, vol. 150, no. 2, Article ID 04024003, 2024.
- [26] A. Jain, G. Hautier, C. J. Moore et al., "A high-throughput infrastructure for density functional theory calculations," *Computational Materials Science*, vol. 50, no. 8, pp. 2295–2310, 2011.
- [27] P. Hohenberg and W. Kohn, "Inhomogeneous electron gas," *Physical Review*, vol. 136, no. 3B, pp. B864–B871, 1964.
- [28] G. Kresse and J. Furthmüller, "Efficient iterative schemes for ab initio total-energy calculations using a plane-wave basis set," *Physical Review B*, vol. 54, no. 16, pp. 11169–11186, 1996.
- [29] P. E. Blöchl, "Projector augmented-wave method," *Physical Review B*, vol. 50, no. 24, pp. 17953–17979, 1994.
- [30] J. P. Perdew, K. Burke, and M. Ernzerhof, "Generalized gradient approximation made simple," *Physical Review Letters*, vol. 77, no. 18, pp. 3865–3868, 1996.
- [31] S. P. Ong, W. D. Richards, A. Jain et al., "Python materials genomics (pymatgen): a robust, open-source python library for materials analysis," *Computational Materials Science*, vol. 68, pp. 314–319, 2013.
- [32] L. Wang, T. Maxisch, and G. Ceder, "Oxidation energies of transition metal oxides within the GGA+ U framework," *Physical Review B*, vol. 73, no. 19, Article ID 195107, 2006.
- [33] A. Jain, G. Hautier, S. P. Ong et al., "Formation enthalpies by mixing GGA and GGA+ U calculations," *Physical Review B*, vol. 84, no. 4, Article ID 045115, 2011.
- [34] A. Jain, S. P. Ong, G. Hautier et al., "Commentary: the materials project: a materials genome approach to accelerating materials innovation," *APL Materials*, vol. 1, no. 1, Article ID 011002, 2013.
- [35] S. P. Ong, L. Wang, B. Kang, and G. Ceder, "Li–Fe–P–O₂ phase diagram from first principles calculations," *Chemistry of Materials*, vol. 20, no. 5, pp. 1798–1807, 2008.
- [36] Y. Zhu, X. He, and Y. Mo, "First principles study on electrochemical and chemical stability of solid electrolyte-electrode interfaces in all-solid-state Li-ion batteries," *Journal of Materials Chemistry A*, vol. 4, no. 9, pp. 3253–3266, 2016.

- [37] A. Ponrouch, D. Tchitchekova, C. Frontera, F. Bardé, M. E. A.-D. Dompablo, and M. R. Palacín, “Assessing Si-based anodes for Ca-ion batteries: electrochemical decalciation of CaSi₂,” *Electrochemistry Communications*, vol. 66, pp. 75–78, 2016.
- [38] R. Pfenninger, M. Struzik, I. Garbayo, E. Stilp, and J. L. M. Rupp, “A low ride on processing temperature for fast lithium conduction in garnet solid-state battery films,” *Nature Energy*, vol. 4, no. 6, pp. 475–483, 2019.
- [39] C. Wang, Y. Gong, B. Liu et al., “Conformal, nanoscale ZnO surface modification of garnet-based solid-state electrolyte for lithium metal anodes,” *Nano Letters*, vol. 17, no. 1, pp. 565–571, 2017.